19th Brazilian Congress of Thermal Sciences and Engineering
November 6th–10th, 2022, Bento Gonçalves - RS - Brazil

ENC-2022-0225
AERODYNAMIC INVESTIGATION OF A MIRA FASTBACK MODEL GEOMETRY USING CFD TECHNIQUES BASED ON EXPERIMENTAL WIND TUNNEL ANALYSIS

Luckyan Kanigoski Quintino
luckyanquintino@gmail.com
Jorge Esteban Chavez Gutierrez
jorge.chavez@labmci.ufsc.br
Leonel R. Cancino
leonel.cancino@labmci.ufsc.br
Internal Combustion Engines Laboratory - Joinville Technological Center - Federal University of Santa Catarina - LABMCI/CTJ/UFSC.
Rua Dona Francisca 8300, Joinville, SC, CEP 89219-600, Brazil.

Abstract. *Aerodynamics is a high applicability type of science, used in the development of energy efficient automobiles and, airplanes, even considered in the design of great infrastructures such as tall buildings and bridges. On the rise of the computer era, computational tools were then developed to calculate the effects of fluid dynamics on virtual bodies without manufacturing a prototype or using a wind tunnel. Experimentalists have been working together, using testbenches as wind tunnels in order to better understand the fluid flow around vehicles. In function of the car shape diversity, it was necessary to define some automotive reference geometries, it means, some geometry that is not actually a car geometry but is a body that can be used to better understand the flow pattern around a real car. In this work, the MIRA reference fastback type model was numerically investigated. Its geometry differs in the rear with a smooth transition between the roofline and the rear end of the body, eliminating the three-volume characteristic of a traditional sedan car body. Mesh and computational domain independence test were then performed to guarantee reliable numerical data. The obtained fluid flow pattern, using the commercial ANSYS FLUENT™ software, is then discussed in terms of aerodynamic behavior and compared to experimental data available at the literature. The set-up was built using wind tunnel experimental data available at the literature. Flow structures like vortices, separation and reattachment were numerically visualized and analyzed. Four turbulence models where then used for numerical simulations: κ - ε Realizable, κ - ε RNG, κ - ω and Reynolds Stress Model were tested to compare and validate the numerical results as well as numerical procedures. The κ - ε Realizable turbulence model shows the better numerical predictions for c_D and c_L, when compared to the experimental data.*

Keywords: *Computational Fluid Dynamics, MIRA fastback body, Aerodynamic behavior, Turbulence model*

1. INTRODUCTION

Nowadays fuel prices had increased considerably, and this kind of situations normally highlight fuel efficient kind of cars. Although a low drag coefficient is possible, it's not always achievable in a car project because of the air flow around the body that also has direct impact in the vehicle stability as well as in noise generation, both vital to the success of the car as a product in safety and comfort categories (Schutz, 2015). It is clear that the along the design of a car, several steps are followed and each one of steps involves several tools, also, it is normal nowadays to hear about the potential of computational fluid dynamics as a main tool in the automotive industry, covering and being applied to several areas in the hole car project: combustion and electrical propulsion systems, powertrain system and aerodynamics (Heywood (2018); Schutz (2015); Merker *et al.* (2012) and references therein). Along this process, experimentalists have been working together, obviously investing big funds applied to testbenches as wind tunnels in order to better understand the fluid flow around vehicles. At the beginning "normal" wind tunnels were then built, today is "normal" to find completely sophisticated wind tunnels trying to, in-laboratory, reproduce the natural ambient of a car, some examples of this kinds of wind tunnels can be found at Schutz (2015). In function of the car shape diversity in the automotive industry, it was necessary to define or create some automotive reference bodies, it means, some geometry that is not actually a car geometry (involving all the complexities) but is a body that can be used to better understand the flow pattern around a real

car. Obviously some main car shape characteristics must be leave in to account in order to define a realizable automotive reference body. For passengers and sportive cars there are two well knowledge references: (i) the Ahmed body (Ahmed *et al.*, 1984) and (ii) the MIRA reference bodies Carr and Stapleford (1986). The Motor Industry Research Association - MIRA reference geometries were developed after production models of the early 80's initially with three rear body type variation: fastback, notchback and estate-back/wagon and were firstly introduced to calibrate wind tunnels using scale models and full-sized models, those geometry also became a great reference for CFD software validation some decades later. The Motor Industry Research Association - MIRA fastback reference car was first presented by Carr and Stapleford (1986) as a simplified vehicular model used for aerodynamics investigations regarding the blockage effects in wind tunnel testing. The fastback model was one of four conceived by Carr and Stapleford (1986) for their studies, the others were the notch-back (very similar to a sedan model), the van or square-back and the pick-up (less used in posthumous studies). All models share the same front-end and lower rear dimensions and geometry and are distinguished by the upper rear geometry only. According to Le Good and Garry (2004), those models' proportions were based on family-sized cars of the early 80's with a final geometry much more similar to the real-world cars than the Ahmed body for example. Le Good and Garry (2004) commented that all the MIRA reference cars had a great contribution on understanding the influence of test section and investigating blowing and suction effects on ground plane boundary layer and its influence on the car's behavior, in helping to refine and calibrate wind-tunnels and also testing numerical CFD.

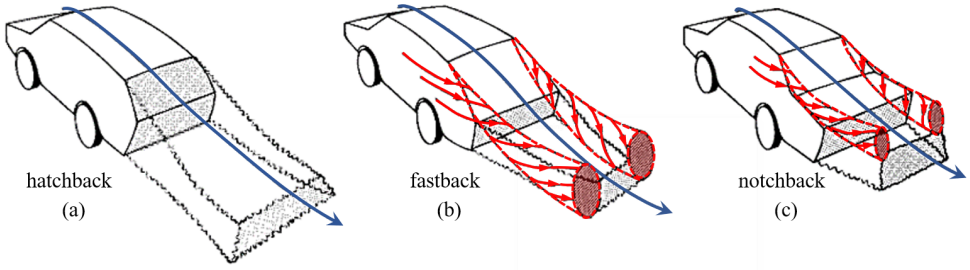

Figure 1. Flow around a car in details - rear body in its variants: (a) hatchback, (b) fastback, and (c) notchback; schematic. Adapted from Schutz (2015)

This study is focused on the analysis of external aerodynamic behavior of the MIRA fastback model geometry using CFD tools. Firstly, the validation of the computational domain independence and later the number of mesh elements independency were done using the κ - ε Realizable turbulence model. After that κ - ε RNG and κ - ω standard were investigated and compared. Schutz (2015) presents some images indicating the wake characteristics according to the rear end of a vehicle (Figure 1(b)), pointing the notchback type design capable of creating short and closed wakes, especially when compared to the hatchback and fastback rear types.

2. EXPERIMENTAL DATA FROM THE LITERATURE

Wang *et al.* (2014) gathered multiple experimental data for the c_D values from the TJ-2 wind tunnel of Tongji University (the MIRA models at the TJ-2 and IVK wind tunnel facilities) and also Hoffman *et al.* (2001) results to compare with their own measurements and CFD analysis. All those values are shown at Table 1, alongside with the c_L data measured by Wang *et al.* (2014)

Table 1. Drag and Lift coefficients of MIRA reference geometries - Experimental data presented by Wang *et al.* (2014)

	HD-2 Wind Tunnel	TJ-2 Wind Tunnel	IVK Wind Tunnel	Hoffman *et al.* (2001) Sim.	CFD Sim.	HD-2 Wind Tunnel	CFD Sim.
Rear body			c_D			c_L	
Fastback	0.2849	0.2631	0.2795	≈0.26	0.2738	0.0460	0.0410
Notchback	0.3183	0.3016	0.3204	≈0.29	0.3048	0.0416	0.0397
Squareback	0.3842	0.3668	0.3874	≈0.36	0.3742	-0.3633	-0.3592

The data presented by Wang *et al.* (2014) includes five different values for the Drag coefficient of the MIRA Fastback with a maximum of 0.2849, measured at the HD-2 wind tunnel (Figure 2), and a minimum of 0.2631 measured at the TJ-2 wind tunnel of Tongji University, presenting a 7.65% difference between themselves. In the other hand, the only reference for lift coefficients presented were those measured by Wang *et al.* (2014)) by experimental and CFD methods. For those reasons, the c_D were chosen as primary reference value to validate the simulations used for mesh and computational domain size independence. Other data were collected in order to have a primary reference over other important parameters

and consequently facilitate the verification of the final results such as the surface pressure on longitudinal symmetry plane and the expected wake structure and air behavior at the rear end of the model. Zhengqi *et al.* (2011) measured the pressure distribution over a MIRA Fastback model at the HD-2 wind tunnel at the Hunan University using 58 m/s as the flow speed input for a 1/3 scale model. Although Zhengqi *et al.* (2011) used the same wind tunnel, model and scale of this paper study, the numeric results for those cases are not directly comparable because of the difference of velocity. But the pressure distribution should be very similar, especially at the front and of the car, considering that Zhengqi *et al.* (2011) were capable of maintaining a laminar flow approaching the frontal area of the model.

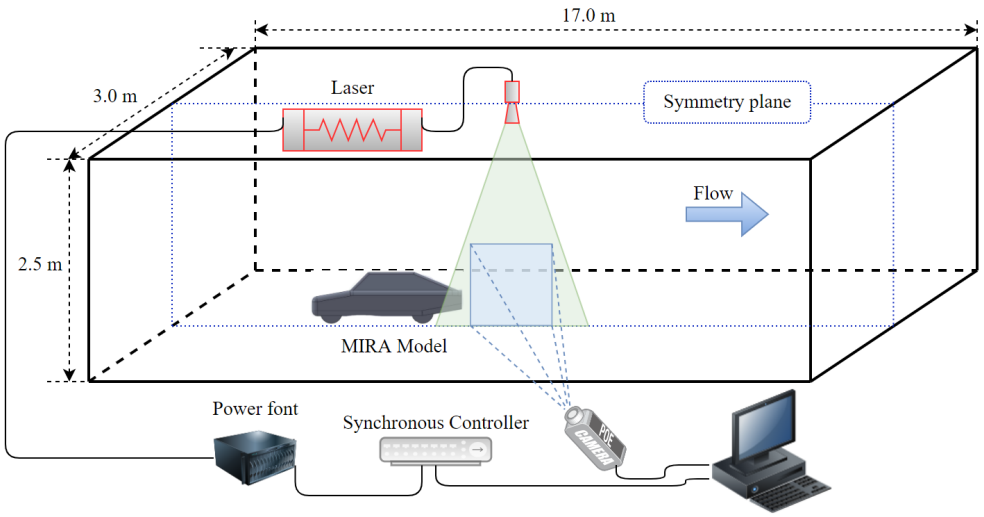

Figure 2. HD-2 Boundary Layer Wind Tunnel (HD-2BLWT) schematic configuration (adapted) used by Wang *et al.* (2014) for PIV measurement

3. METHODOLOGY

3.1 The MIRA fastback geometry used in this work

The MIRA fastback reference car used for the CFD analysis is very similar to the model used by Wang *et al.* (2014) on their wind tunnel experiment: an 1:3 scale model respecting mostly dimensions. Some angles and dimensions were not informed by Wang *et al.* (2014) and therefore were gathered from Carr and Stapleford (1986) for the same scale and also from the Zhang *et al.* (2019) paper, converting the last missing dimensions to 1:3 scale. The body dimensions are informed in Figure 3 below

Other modifications were necessary due some ANSYS FLUENT™ limitations when setting the enclosure as the control volume of the wind tunnel. An error occurred when a symmetry plane was set to limit the volume under the car, as it could not put the wheels of the model in contact with the ground due a tangential condition. The solution applied is shown at Detail A of Figure 3, which consisted in modifying the wheels geometry in order to create a flat surface and eliminate the single line tangential contact. This solution was chosen over other two alternatives, because it resulted later in a better meshing skewness. Although this modification deviates a bit from the original MIRA body design, it could be interpreted as tire deformation effects due vertical load, a regular behavior for a pneumatic tire according to Wong (2001). In this case the main contributor is the body weight. The frontal area calculated for this 1:3 MIRA model equals 0.20637 m^2.

The fluid domain was created in ANSYS Design Modeler™ using the enclosure tool and based on the HD-2 Boundary Layer Wind Tunnel (HD-2BLWT) in Wind Engineering Research Center, Hunan University, same used by Wang *et al.* (2014) and shown at Figure 2. Using the model's origin location as reference it was possible to apply symmetry conditions to the enclosure tool at XZ and YZ planes, which resulted in a half car model with the wheels touching the floor. The total height of the virtual wind-tunnel was set as 2.5 m, and the total width set as 1.5 m due to the symmetry condition applied in the YZ plane, both representing the dimensions of the HD-2 tunnel. Since there are no clear indications of the position of the model along the length of the wind tunnel, the distance between the velocity inlet and the model most forward point was set following the recommendations of Agarwal (2013) work, which suggests a length of 3 times of the model length ahead of it, and therefore this dimension was defined as 4167 mm. A convergence test on the tunnel rear length were executed, using 8, 10, 12 and 14 times the model total length for the distance between the model's most rearward point and the pressure outlet. Smaller lengths were not used in this comparison, because they are more likely to produce questionable results as showed by Gutierrez *et al.* (2020).

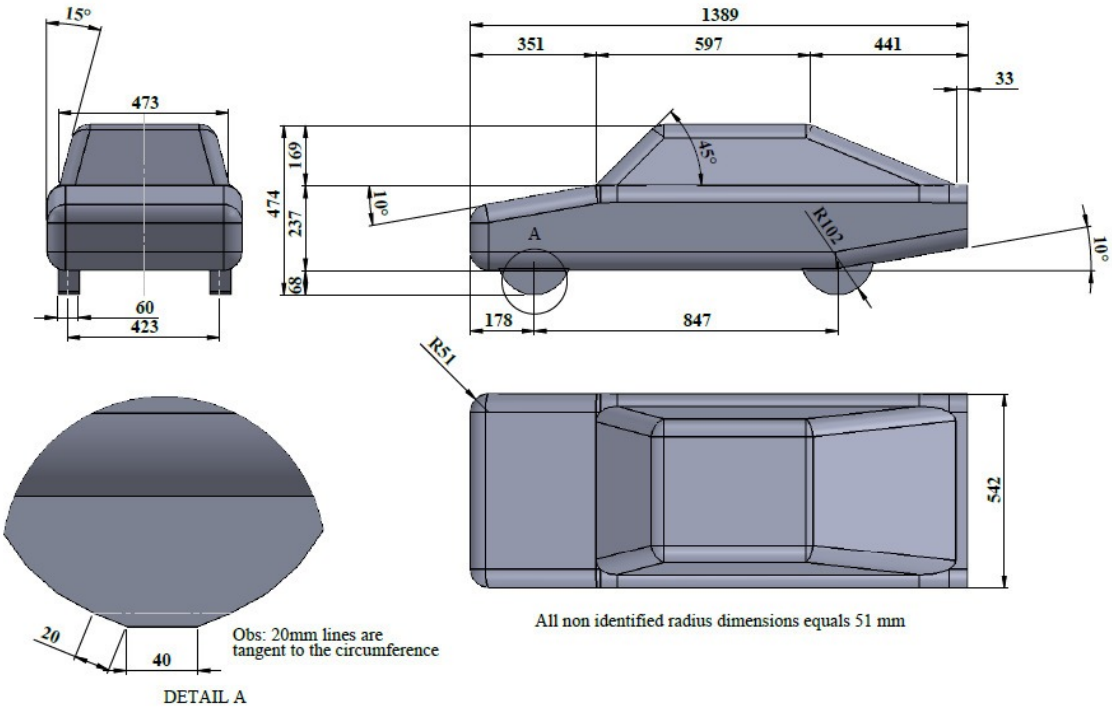

Figure 3. MIRA Fastback reference car dimensions in mm

3.2 Meshing procedures and Boundary conditions

Three boxes were created near the car in order to increase meshing refinement in their respective regions. The boxes are shown below in the Figure 4:

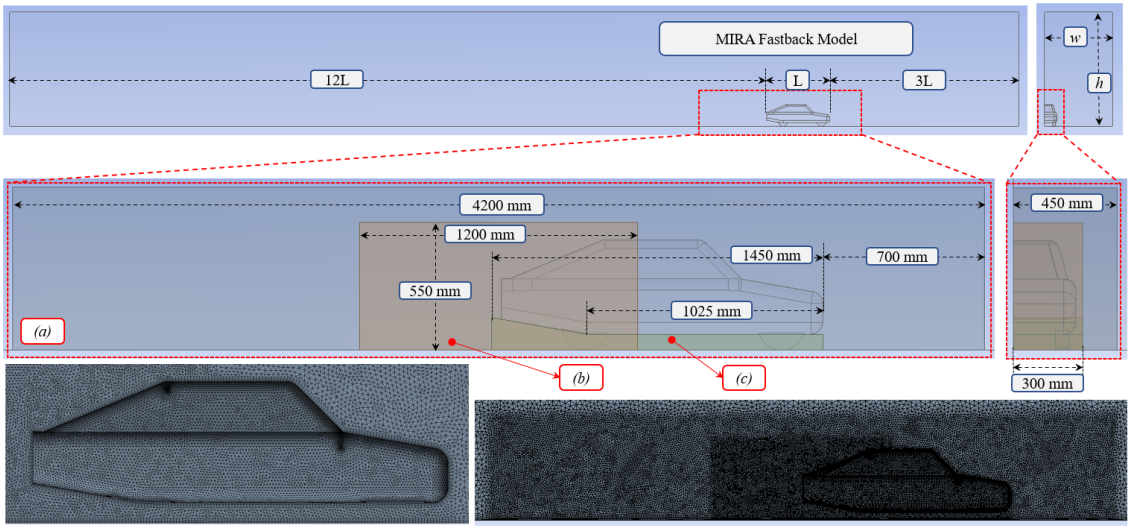

Figure 4. Dimensions of virtual wind tunnel and the boxes *(a)* Carbox, *(b)* Wakebox, *(c)* Underbox for mesh refinement purposes. The *w* and *h* correspond to the real wind tunnel used by Wang *et al.* (2014) (see Figure 2), and " L " represents the MIRA fastback length = 1389 mm.

The carbox (Figure 4*(a)*) and the Underbox (Figure 4*(c)*) used fixed parameters for all the executed simulations, the first one used 15 mm and the second one used 10 mm mesh sizing. Both boxes were configurated as body of influence for each respective sizing over the full computational domain. The Wakebox (Figure 4*(b)*) used different sizing for the simulations, because it was the variable modified for the mesh convergence test. Other two special refinements were applied to the domain, one using the faces of the MIRA Fastback model as reference for a 10 mm sizing and a special 5 mm sizing applied only to the wheels of the model. Both sizing were configured with a soft behavior. Mesh Defeaturing was set active alongside with Capture Curvature with 12° of normal angle and Capture Proximity for faces and edges.

The remaining parameters for the mesh generation process were kept as default values.

3.3 Simulation set-up

Figure 5 shows kinds of boundary conditions used in this work for all the simulations. The velocity inlet was set to 20 m/s according to Wang *et al.* (2014) experiments, and since this value is under Mach 0.3, allowing the despise of compressibility effects (Cengel and Cimbala, 2017). With this consideration, a pressure-based solver was selected being the most adequate solver for incompressible flows at low velocity due also to its capacity to operate at low Mach numbers, (Mangani *et al.*, 2016).

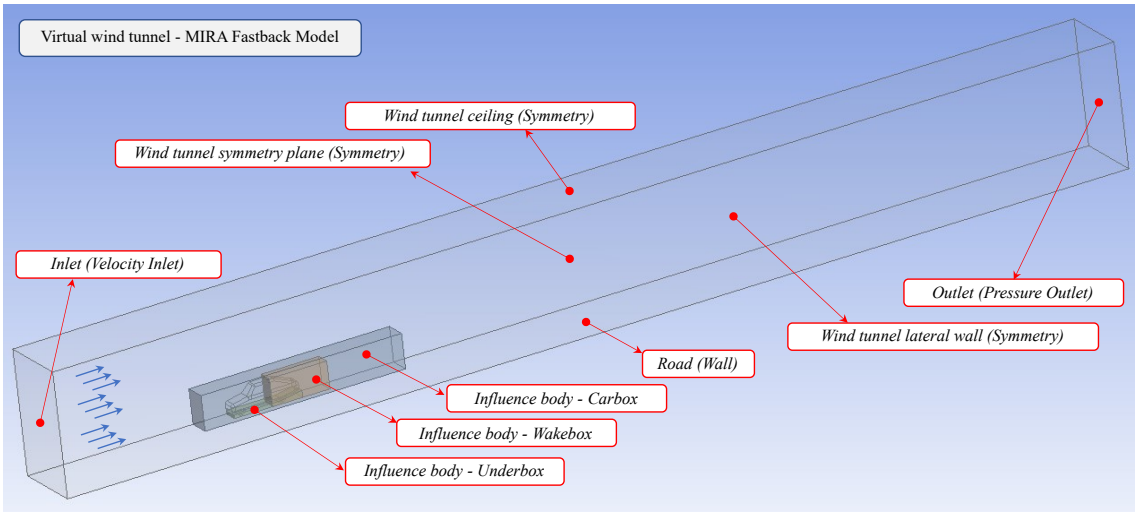

Figure 5. Boundary conditions used in this work for all the simulations

The use of a turbulence model is necessary to approach the solution achieved in experimental analysis. For this reason, the simulations of this project were developed with three turbulence models: κ - ε Realizable, κ - ε RNG and κ - ω Standard, being the first model used for the independence tests and also used by Wang *et al.* (2014) simulation. A hybrid initialize method was selected, using the default parameters for 10 iterations. Following the initialization, 100 iterations using first order upwind equations for momentum, turbulent dissipation rate and turbulent kinetic energy were executed and after conclusion those parameters were changed to second order equations and the turbulence viscosity modified to 0.95 set to iterate until achieving a convergence status. The coupled pressure-velocity method were selected, using a least squares cell based gradient and standard pressure. The inlet was configured with 1% of turbulent intensity and a ratio of 10 for the turbulent viscosity. The outlet set to prevent reverse flow with 0.0 Pa of gauge pressure, 5% of backflow turbulent intensity and a ratio of 10 for the backflow turbulent viscosity. The floor (road) and the model were considered as no slip stationary walls, and the remaining faces considered as symmetry. The viscous model for the κ - ε Realizable considered non-equilibrium wall functions, C2-ε as 1.9, TKE and TDR Prandtl Number equal to 1 and 1.2 respectively. All the values for boundary conditions were obtained from the literature at similar flow configurations (Lanfrit (2005); Gutierrez *et al.* (2020); Zhang *et al.* (2019); Wilcox (1994) and references therein)

All the simulations were initially set to iterate until the residual values of all the transport variables decreased below $1x10^{-4}$, unfortunately the continuity residual was reducing very slowly after 600 iterations, so a target of at least 1000 iterations were set, and if the other residual values were below $1x10^{-4}$, than the simulation was considered convergent. Before testing others turbulence models, two independence tests were performed using the κ - ε Realizable turbulence model: one varying the computational domain size and the other varying the mesh sizing at the Wakebox.

4. RESULTS AND DISCUSSION

In this section, all the numerical results of this work are presented. For all the simulations, convergence was considered “acceptable" when the residuals of all the transport variables were below $1x10^{-4}$. In order to identify the virtual tunnel length and the minimum mesh size, two independence test where then performed. The virtual tunnel cross section area is the same as in the experimental procedures of Wang *et al.* (2014), resulting in a blockage ratio of $\approx$2.75% which meets the requirement that the blockage ratio of the experimental model should be less than 5% (Choi and Lee, 2000). Four turbulence models where then used in order to identify the “ strong and weak " points of each turbulence model for road vehicle aerodynamics under the flow conditions of this work.

4.1 Computational domain length and Mesh size independence tests

The distance from the rear surface of the MIRA Fastback reference geometry to the exit of the numerical wind tunnel (12L in the upper part of Figure 4) was defined for domain length independence analysis. To develop this study, the rear length [L] was varied between 8L and 14L, where L denotes the total length of the MIRA fastback length geometry (1389 mm), as shown in Figure Figure 4. On the other hand, the same dimensions and refinement parameters were maintained for the underbody-box and car-box influence volumes (Figure 4), while the dimensions and refinement parameters of the wake-box were varied proportionally with the back length of the computational domain, this means that the size of this volume of influence was varied as the study of independence of the length of the computational domain was executed, once this length was defined, the study of mesh independence test was carried out. The drag coefficient c_D was selected to analyze the convergence and independence criteria. Figure 6 shows the results of independence test performed in this work.

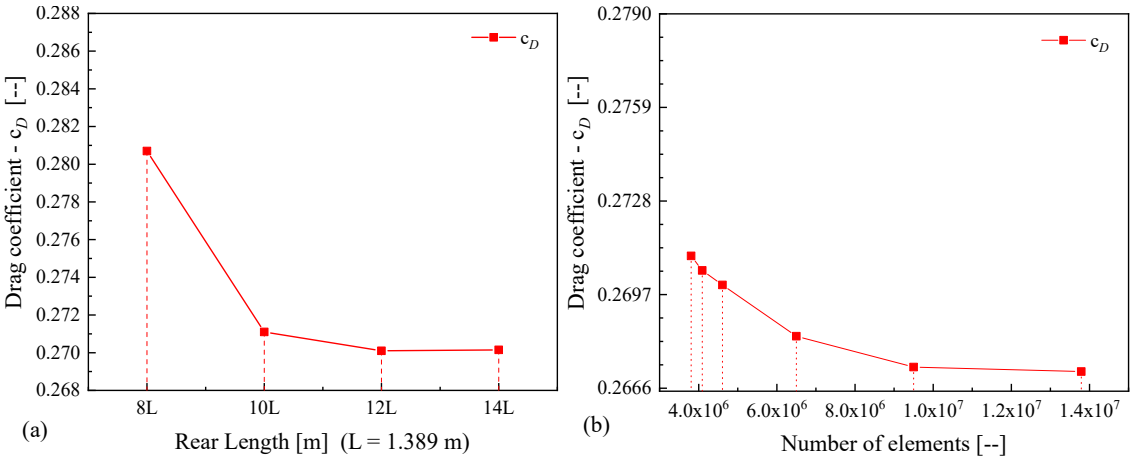

Figure 6. Computational domain length and Mesh size independence tests.

The train observed in Figure 6(a) indicates that for rear length bigger that 12L no significant c_D variation is elucidated, of this form, the rear length of 12L was selected for numerical simulations from this point and forward. The Figure 6(b) shows the mesh size independence test results, here is possible to observe that for a mesh with a elements number among $1.0x10^7$ and $1.4x10^7$ there is no c_D representative variation. The final computational mesh used for analysis in this work has 13'790.730 elements and the rear length is 12L (Figure 4)

4.2 Drag, lift and pressure coefficients

The methodology described for the preparation of the CFD simulation were reproduced using different turbulence models, those were the κ - ω and the Reynolds Stress Model (RSM). The κ - ε RNG model were also simulated, but the convergence parameters for the residual values were not fulfilled, consequently those results will not be presented. The final values calculated for c_D and c_L are displayed at Table 2 below:

Table 2. Drag and Lift coefficients calculated for different turbulence models

	This work			Wang *et al.* (2014)	
Aerodynamic Coefficient	Numerical κ - ε realizable	Numerical κ - ω	Numerical RSM	Experiment HD-2 Wind Tunnel	Numerical κ - ε realizable
c_D	0.2671	0.2814	0.3214	0.2849	0.2738
c_L	0.0381	0.0890	0.0596	0.0460	0.0410

All the turbulence models resulted in quite distant values from those from the Wang *et al.* (2014) reported in their paper and none of them could match precisely the values for both c_D and c_L. The κ - ε Realizable turbulence model presented the closest result for lift, with 7% difference to the Wang *et al.* (2014) CFD results and 17% for the experimental results. The other two turbulence models simulated resulted in considerably distant lift values, being the experimental coefficient 30% less than the indicated by the Reynolds Stress Turbulence model (RMS) simulation and 94% to the κ - ω turbulence model simulation. In relative comparison, the difference between the κ - ω and RSM to the Wang *et al.* (2014) lift coefficient is considerably big, but confronting the values directly the difference stands in 10^{-2} order, being this the same

order of magnitude, thus the high percentage differences between values. The drag coefficients in the other hand are closer to the results registered by Wang *et al.* (2014), being κ - ω the more accurate turbulence model with only 1% less than the experimental value an 3% more than the CFD results obtained by Wang *et al.* (2014). The κ - ε Realizable turbulence model also presented a good result with only 2% difference to the CFD results and 6% to the experimental results. The RSM turbulence model presented the worst results compared to the values of drag presented by Wang *et al.* (2014) and also the highest, being 13% bigger than the experimental and 17% bigger than the CFD results.

The results of this study over drag and lift indicates that the κ - ε Realizable is the best turbulence model to reproduce Wang's wind tunnel experiment when analyzing both drag and lift together. If the focus of the simulation go only towards the drag parameters the κ - ω turbulence model is the best choice, but analyzing any other lift dependent parameter like the aerodynamic balance, it becomes a bad choice, since its results shown a high inaccuracy regarding the lift coefficient. Lastly, the RSM model also seems not to be a suitable turbulence model for this study, not only because the results obtained for both drag and lift coefficients are not accurate with the data presented by Wang *et al.* (2014) for the same experiment condition, but also because this model demands much more computational capacity for the calculations. This means that, for the same computer, the final results would take longer to be achieved when compared to the other turbulence models.

Figure 7 shows the pressure coefficient contours in the MIRA fastback geometry surface. The rear angle in this geometry is about 22.5°, it means below the critical angle ($\sim 30°$) related to automotive fastback geometries (Hucho, 1998), of this form, the MIRA fastback geometry analyzed in this work must return a low drag coefficient, as explained by Ahmed *et al.* (1984) using the classical Ahmed body reference geometry.

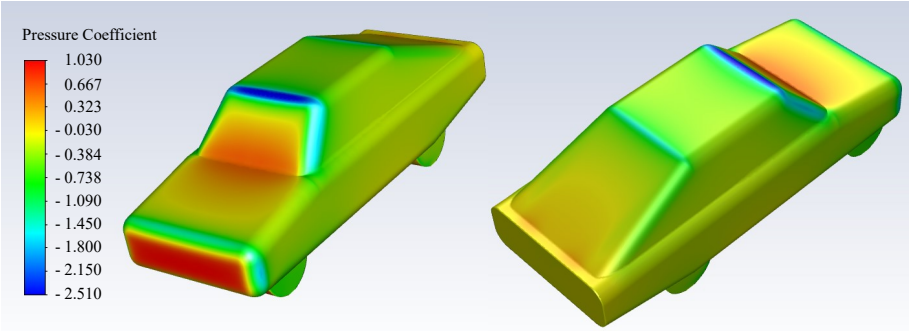

Figure 7. Pressure coefficients - Numerical prediction using the κ - ε Realizable turbulence model.

4.3 Flow field

The flow field obtained using the κ - ε turbulence model is very close to the results presented by Wang *et al.* (2014) for the fastback model. Figure 8(a) below shows the pathlines in the symmetry plane around the body. Than pathlines indicates the formation of two vortex structures, a clockwise vortex coming from the upper flow and an anti-clockwise vortex formatted by the air flow under the body, as mentioned in the classical work of Ahmed *et al.* (1984) for fastback reference geometry.

The pathlines also shows that part of the upper airflow changes its trajectory in a limit line between the two generated vortex structures centers, helping both the vortex to grow instead of only contributing to the expansion of the clockwise vortex. Another parameter analyzed were the wind velocity magnitude (Figure 8(b)) around the body at the symmetry plane. Focusing at the rear part of the body its possible to see a stagnation region, where the velocity values are very close to zero. It is also possible to observe a high velocity region formed under the body due to the Venturi effect, consisting in the acceleration of the airflow due to a transversal area expansion. In order to better understand the wake structure, 6 different planes behind the car body showing the pathlines are then plotted on Figure 9 (planes equivalents to Wang *et al.* (2014) X/L 0.6 to 1.1 - (b) $X/L = 0.6$, (c) $X/L = 0.7$, (d) $X/L = 0.8$, (e) $X/L = 0.9$, (f) $X/L = 1.0$, and (g) $X/L = 1.1$). That figure shows the vortex structures as depicted in the literature (Ahmed *et al.*, 1984; Hucho, 1998; Gutierrez *et al.*, 2020; Schutz, 2015)

Illustratively, a simple comparison of Figure 9(a) to Figure 1(b) can elucidate the weak flow structure, predicted for fastback reference geometries (Schutz, 2015; Hucho, 1998). In this work, all the turbulence model tested (κ - ε Realizable, κ - ε RNG, κ - ω and Reynolds Stress Model) shows that behavior, even the κ - ε RNG turbulence model with residuals around 10^{-2}. Additionally, both the vortices at the rear (Figure 8(a) also were reproduced for all turbulence models used in this work, however, with different shapes. Figure 9(a) shows that two vortices for the numerical prediction using the κ - ε Realizable turbulence models. Results for the other turbulence models used in this work are not exhibited because of the big quantity of data. Figures 9 (b) to (g) shows the sequence of six planes ((b) $X/L = 0.6$, (c) $X/L = 0.7$, (d) $X/L = 0.8$, (e) $X/L = 0.9$, (f) $X/L = 1.0$, and (g) $X/L = 1.1$) illustrating the pair of trailing 3D vortices formed in the C-pillars of the MIRA fastback geometry.

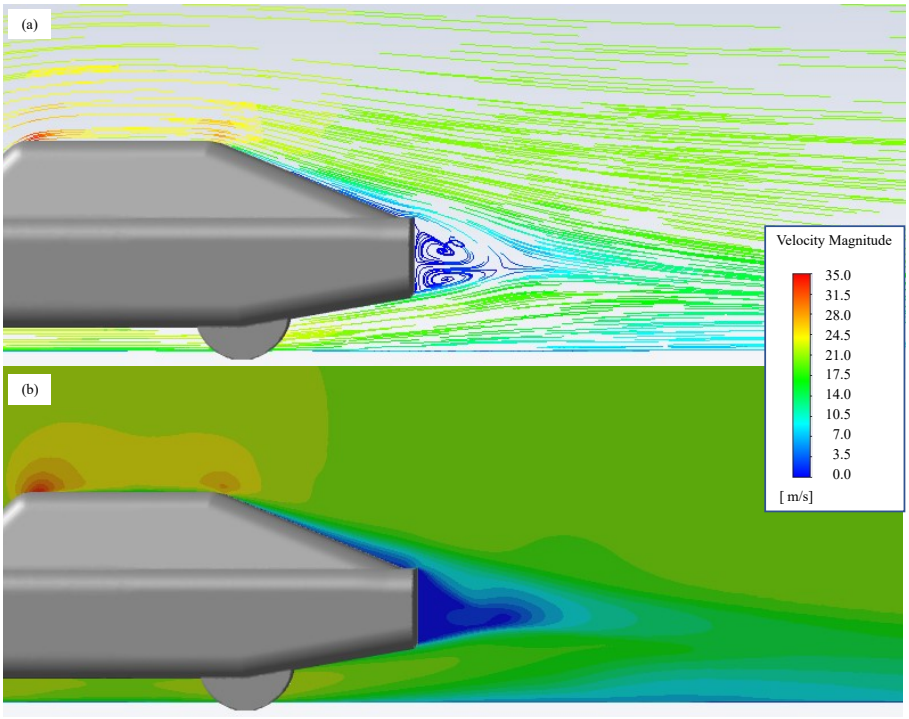

Figure 8. (a) Pathlines colored by velocity magnitude. (b) Velocity contours. Symmetry plane - Numerical prediction using the κ - ε Realizable turbulence model.

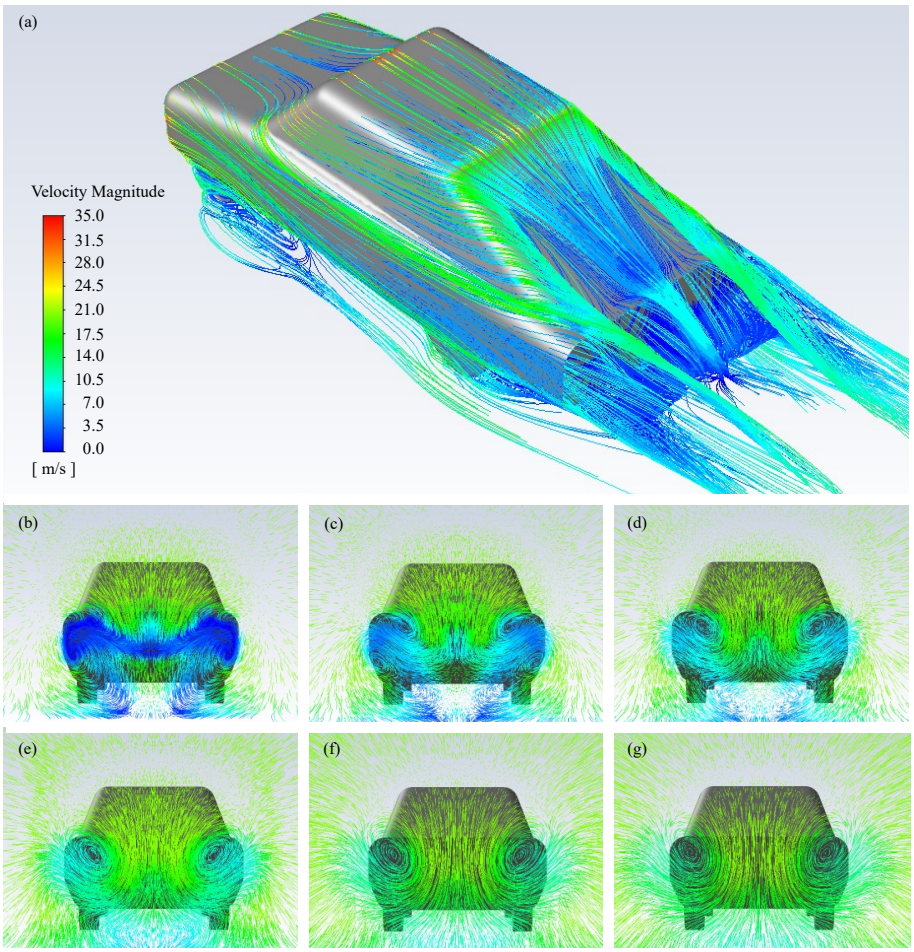

Figure 9. Path lines colored by velocity - Numerical prediction using the κ - ε Realizable turbulence model.

The turbulent kinetic energy (κ) was also plotted in the same six planes, ((b) X/L = 0.6, (c) X/L = 0.7, (d) X/L = 0.8, (e) X/L = 0.9, (f) X/L = 1.0, and (g) X/L = 1.1), Figure 10 below show these results. The work from Wang *et al.* (2014) reports experimental and numerical data of turbulent kinetic energy (κ), with maximum levels of $\kappa \sim$45 m^2/s^2 (Figure 19(a) in the Wang *et al.* (2014) paper), in this work, the maximum turbulent kinetic energy (κ) numerical data was around $\kappa \sim$35 m^2/s^2. Here is necessary to inform that the comparison of turbulent kinetic energy (κ) maximum levels is done at the same turbulence model (κ - ε Realizable) and boundary conditions.

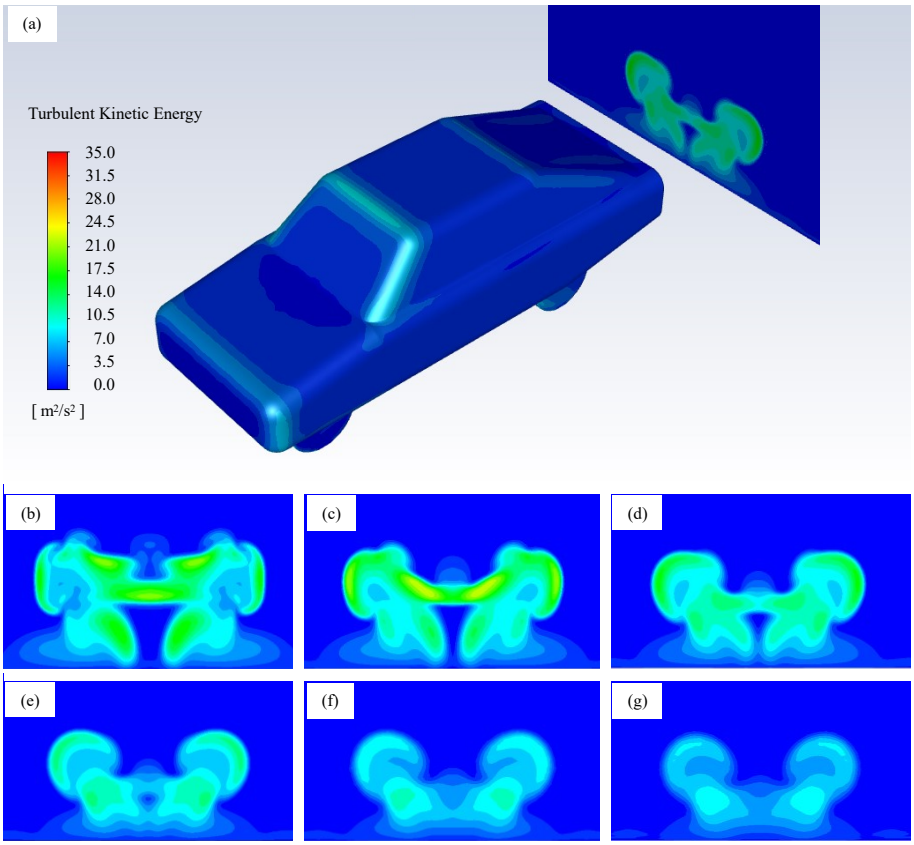

Figure 10. Turbulent Kinetic Energy - Numerical prediction using the κ - ε Realizable turbulence model.

5. CONCLUSION

The experience of reproducing a wind tunnel experiment exploring other difference models involved several steps, including the validation of the parameters such as mesh and computational domain independence, the calculation itself and the critical analysis of the results. All the best practices recommended for CFD studies were also applied during the pre-processing stage until the conclusion of the calculation, example given: the fulfillment of the convergence criteria for the residual parameters in order to raise the simulation results credibility. Comparing the simulated models, the κ - ε Realizable has an evident benefit towards the others, because it could reproduce the experimental values acceptable precisely consuming a lower computational power. In this work, the ANSYS-FLUENT™ CFD software was used for numerically analyze the aerodynamic response of the MIRA fastback reference automotive geometry. Along the numerical procedure, independence tests (domain length and mesh size) were conducted in order to obtain reliable numerical data with less (or without) influence of the dimensions used in the problem description and discretization. In this way, the external aerodynamics of the reference geometry was then analyzed and understood. The Reynolds Stress Model shows a poor behavior in this work, maybe related to the mesh quality refinement, however, is well knowledge that RSM model usually performs better for vehicular aerodynamics (Hucho, 1998; Gutierrez *et al.*, 2020; Schutz, 2015), specially for lift prediction. The κ - ε Realizable turbulence model presented the closest result for lift, difference of 17% to the experimental results of Wang *et al.* (2014). The other two turbulence models simulated resulted in considerably different lift values, being the experimental coefficient 30% less than the indicated by the Reynolds Stress Turbulence model (RMS) simulation and 94% to the κ - ω turbulence model simulation. The drag coefficients in the other hand are closer to the results registered by Wang *et al.* (2014), being κ - ω the more accurate turbulence model with only 1% less than the experimental value an 3% more than the CFD results obtained by Wang *et al.* (2014). The κ - ε Realizable turbulence model also presented a good result with only 2% difference to the CFD results and 6% to the experimental results. The

RSM turbulence model presented the worst results compared to the values of drag presented by Wang *et al.* (2014) and also the highest, being 13% bigger than the experimental and 17% bigger than the CFD results. The κ - ε RNG turbulence model does not show convergence below 10^{-4} and of this form its results were not presented in this work.

6. ACKNOWLEDGEMENTS

The authors would like to acknowledge the support of UFSC Joinville TI team (Mr. Kleber Carlos Francisco) for all support given to the LABMCI computer network.

7. REFERENCES

Agarwal, R., 2013. "Sustainable Ground Transportation: Technologies, Challenges and Opportunities". American Society of Mechanical Engineers Digital Collection. doi:10.1115/ES2013-18028.

Ahmed, S.R., Ramm, G. and Faltin, G., 1984. "Some Salient Features of the Time -Averaged Ground Vehicle Wake". *SAE Transactions*, Vol. 93, pp. 473–503. ISSN 0096-736X. URL https://www.jstor.org/stable/44434262. Publisher: SAE International.

Carr, G.W. and Stapleford, W.R., 1986. "Blockage Effects in Automotive Wind-Tunnel Testing". p. 860093. doi: 10.4271/860093. URL https://www.sae.org/content/860093/.

Cengel, Y. and Cimbala, J., 2017. *Fluid Mechanics: Fundamentals and Applications*. McGraw Hill, New York, NY, 4th edition. ISBN 978-1-259-69653-4.

Choi, J.H. and Lee, S.J., 2000. "GROUND EFFECT OF FLOW AROUND AN ELLIPTIC CYLINDER IN A TURBULENT BOUNDARY LAYER". *Journal of Fluids and Structures*, Vol. 14, No. 5, pp. 697–709. ISSN 0889-9746. doi:10.1006/jfls.2000.0290.

Gutierrez, J.E.C., Duarte, L.E.D., Oliveira, A.A.M. and Cancino, L.R., 2020. "The Ahmed Body's External Aerodynamics at 25° Slant Angle Rear Surface: A Numerical Analysis Using CFD". In *Proceedings of the 18th Brazilian Congress of Thermal Sciences and Engineering*. pp. ENC–2020–0060. URL https://repositorio.ufsc.br/bitstream/handle/123456789/217969/ENCIT2020-0060-JECGutierrez.pdf?sequence=1&isAllowed=y.

Heywood, J.B., 2018. *Internal Combustion Engine Fundamentals 2E*. McGraw-Hill Education, 2nd edition. ISBN 978-1-260-11610-6.

Hoffman, J., Martindale, B., Arnette, S., Williams, J. and Wallis, S., 2001. "Effect of Test Section Configuration on Aerodynamic Drag Measurements". pp. 2001–01–0631. doi:10.4271/2001-01-0631.

Hucho, W.H., ed., 1998. *Aerodynamics of Road Vehicles: From Fluid Mechanics to Vehicle Engineering*. Sae Intl, Warrendale, PA, 4th edition. ISBN 978-0-7680-0029-0.

Lanfrit, M., 2005. "Best practice guidelines for handling Automotive External Aerodynamics with FLUENT".

Le Good, G.M. and Garry, K.P., 2004. "On the Use of Reference Models in Automotive Aerodynamics". pp. 2004–01–1308. doi:10.4271/2004-01-1308. URL https://www.sae.org/content/2004-01-1308/.

Mangani, L., Sanz, W. and Darwish, M., 2016. "Comparing the performance and accuracy of a pressure based and a density-based coupled solver". In *Proceedings of the International Symposium on Transport Phenomena and Dynamics of Rotating Machinery*. ISROMAC 2016, Hawaii, Honolulu, pp. hal–01894391. URL https://hal.archives-ouvertes.fr/hal-01894391/document.

Merker, G.P., Schwarz, C. and Teichmann, R., eds., 2012. *Combustion Engines Development - Mixture Formation, Combustion, Emissions and Simulation*. Springer-Verlag, Berlin Heidelberg. ISBN 978-3-642-02951-6.

Schutz, T., ed., 2015. *Aerodynamics of Road Vehicles*. SAE International, Warrendale, Pennsylvania, 5th edition. ISBN 978-0-7680-7977-7.

Wang, Y., Xin, Y., Gu, Z., Wang, S., Deng, Y. and Yang, X., 2014. "Numerical and Experimental Investigations on the Aerodynamic Characteristic of Three Typical Passenger Vehicles". *Journal of Applied Fluid Mechanics*, Vol. 7, No. 4, pp. 659–671. ISSN 1735-3572. doi:10.36884/jafm.7.04.21460.

Wilcox, D.C., 1994. *Turbulence Modeling for CFD*. DCW Industries, Inc., La Cañada, California. ISBN 0-9636051-0-0.

Wong, J.Y., 2001. *Theory of Ground Vehicles, 3rd Edition*. Wiley-Interscience, New York, 3rd edition. ISBN 978-0-471-35461-1.

Zhang, Y., Zhang, J., Wu, K., Wang, Z. and Zhang, Z., 2019. "Aerodynamic Characteristics of Mira Fastback Model in Experiment and CFD". *International Journal of Automotive Technology*, Vol. 20, No. 4, pp. 723–737. ISSN 1976-3832. doi:10.1007/s12239-019-0068-x.

Zhengqi, G., Wang, S., Qiu, J., Zhang, Q., Hu, P. and Chen, X., 2011. "Wind Tunnel Tests of MIRA Model Group for Study of Vehicle's Rear Shape". *Science & Technology Review*. doi:10.3981/j.issn.1000-7857.2011.08.011. URL http://en.cnki.com.cn/Article_en/CJFDTOTAL-KJDB201108023.htm.

8. RESPONSIBILITY NOTICE

The authors are solely responsible for the printed material included in this paper.